NANO LETTERS

2007
Vol. 7, No. 7
1898−1907

# 3D Electron Microscopy Study of Metal Particles Inside Multiwalled Carbon Nanotubes

**Ovidiu Ersen,[†] Jacques Werckmann,[†] Matthieu Houllé,[‡] Marc-Jacques Ledoux,[‡] and Cuong Pham-Huu*[,‡]**

*Institut de Physique et Chimie des Matériaux de Strasbourg, UMR 7504 CNRS-ULP, 23 rue du Loess, 67087 Strasbourg, France, and Laboratoire des Matériaux Surfaces et Procédés pour la Catalyse, UMR 7515 CNRS-ULP, European Laboratory of Catalysis and Surface Sciences (ELCASS), 25 rue Becquerel, 67087 Strasbourg, France*

*Received March 6, 2007; Revised Manuscript Received May 4, 2007*

**ABSTRACT**

**The location of palladium nanoparticles on and inside the multiwalled carbon nanotubes channel is presented for the first time using electron tomography (3D TEM). The palladium salt precursor was rapidly sucked inside the nanotube channel by means of capillarity that is favored by the hydrophilic character of the tube wall after acidic treatment at low temperature. Statistical analysis indicates that the palladium particles were well dispersed and the palladium particle size was relatively homogeneous, ranging from 3 to 4 nm regardless of their location within the nanotube, within the resolution limit of the technique for our experimental conditions, i.e., about 2 nm. Three-dimensional TEM analysis also revealed that introduction of foreign elements inside the tube channel is strongly influenced by the diameter of the tube inner channel, i.e., easy filling seems to occur with a tube channel ≥30 nm , whereas with tubes having a smaller channel (<15 nm), almost no filling by capillarity occurred leading to the deposition of the metal particles only on the outer wall of the tube.**

**Introduction.** Carbon nanotubes (CNTs) have received ever-increasing scientific and industrial interest during the past few years due to their exceptional physical and chemical properties that render them suitable for numerous potential applications ranging from living matter structure manipulation to nanometer-sized computer circuits.[1−4] Carbon nanotubes are formed by rolling graphene sheets with an open tubular channel. The diameter of the tubular channel can vary from few nanometers to several dozen depending on the nature of the synthesis method, i.e., arc-discharge, laser ablation, or catalytic chemical vapor deposition (CCVD).[4−7] Carbon nanotubes usually exhibit an extremely high aspect ratio (length-to-diameter ratio) ranging from 30 to more than many thousands.[8]

It was expected that the tubular morphology and the high aspect ratio of these carbon nanotubes could induce peculiar properties of materials trapped inside the tube.[9,10] In the wake of their discovery, several attempts have been focused on the introduction of foreign elements inside their empty tubule with a hope of generating new composite materials with atypical properties.[11,12] The nanoparticles or nanowires structures hosted inside the carbon nanotubes channel could also be safely protected from the surrounding atmosphere by the carbon nanotube wall, i.e., oxidation, which might be crucial for their subsequence uses. Carbon nanotubes with open ends display highly attractive capillarity properties that allow them to be filled with several elements. The filling is based on the low surface tension of the liquid with respect to carbon nanotube and capillarity forces, which are the driving forces aspirating the liquid into the nanotube channel.[13]

The tube filling can be conducted in different ways: (i) high-temperature filling during the arc-discharge synthesis. In this method, the filling was obtained by drilling the graphite rod for the anode and filling it with a mixture of graphite and a chosen foreign element in a powder form.[14] The tubes were generated along with simultaneous filling by the doped element. In such a method, the major drawback is the inability to control the size of the filled material, which generally has a nanowire morphology unusable for catalysis. (ii) The second method is based on the use of pre-existing carbon nanotubes, either with open or closed caps. The tubes were opened by oxidation, while the filling is conducted either by physical or chemical techniques. In this technique, the tubes are treated in refluxing nitric acid containing a soluble metal salt for various durations.[15,16] The acidic

* Corresponding author. E-mail: cuong.lcmc@ecpm.u-strasbg.fr.
[†] Institut de Physique et Chimie des Matériaux de Strasbourg.
[‡] Laboratoire des Matériaux Surfaces et Procédés pour la Catalyse.

10.1021/nl070529v CCC: $37.00 
**Published on Web 06/14/2007**

solution containing nitrate salt allows the opening of the tube tip and subsequent filling through capillarity. The filling can also be achieved by stirring nanotubes with open ends in a concentrated solution containing nitrate salts.[17] Ensuing reduction led to the formation of discreet metal nanoparticles along the tube channel with diameter similar to the one of the tube channel. Open nanotubes could also be directly filled by capillarity with molten media having a surface tension lower than 100−200 $mN \cdot m^{-1}$, as established by Ebbesen.[18] These techniques are proven to be efficient for filling tubes with relatively small inner diameter. The main drawback is the need of prolonged acidic reflux treatment or the use of molten media and the low selectivity toward deposition of small metal particles inside the tube channel. (iii) Aqueous filling of the nanotubes by capillarity under mild conditions and at room temperature using a low surface tension liquid ($<200$ $mN \cdot m^{-1}$). This latter method allows the selective deposition of the foreign element either in a dispersed morphology (particles size ranging from 2 to 20 nm) for a catalysis field or in nanowire morphology for other applications. Using this method, Pd particles with nanometers size were successfully deposited in multiwalled carbon nanotubes[19,20] or $CoFe_2O_4$ nanowires cast inside a carbon nanotube tubule were formed at relatively low temperature (from an homogeneous aqueous solution of cobalt and iron nitrates) compared to the one usually observed without the presence of carbon nanotubes.[22,23] The most attractive aspects of this last filling method are its simplicity and its ease for scaling up.

Recent reports dealing with the use of the active metallic phase dispersed inside the inner channel of carbon nanotubes have shown interesting properties in several catalytic processes going from gas-phase to liquid-phase reactions, i.e., liquid-phase hydrogenation of cinnamaldehyde and gas-phase selective oxidation of $H_2S$ into elemental sulfur.[19,21,24,25] In addition, the complete absence of microporosity in the carbon nanotubes makes them very attractive compared to the traditional activated charcoal support in which the large number of micropores greatly increases the diffusion phenomena, especially in liquid-phase processes where the diffusion limitation could be several orders of magnitude higher than in the gas-phase reactions. The nanoscopic size of the carbon nanotubes also allows them to overcome attrition problems under vigorous stirring, which is frequently encountered with liquid-phase reactions.

The most popular characterization technique for the study of elements trapped inside carbon nanotubes is the transmission electron microscopy (TEM), which delivers a first insight of the particle size and morphology provided by 2D projections of the solid structure. Nevertheless, the real location and morphology of the deposited foreign elements are not fully established due to the 2D character of traditional TEM images that are in fact projections of a 3D solid structure.

De Jong and co-workers have pioneered the use of electron tomography (here referred as 3D TEM) in the material field to characterize the morphology and location of small metal particles deposited inside zeolites or mesoporous networks.[26−28] The authors used bright-field (BF) mode to obtain the 2D images for volume reconstruction of the sample. Midgley et al.[29,30] have used a high-angle annular dark-field (HAADF) mode based on scanning transmission electron microscopy (STEM) to acquire the 2D projection series for 3D analysis. Another imaging mode that has been recently demonstrated to be suitable for tomographic analysis is energy-filtered TEM (EFTEM).[30−33] This technique allows generation of 3D elemental maps by selecting electrons that have undergone characteristics energy losses, but its application is still limited because of the high electron doses involved in acquisition. The obtained results have opened a new field for investigating the microstructure of solid materials with high spatial resolution that could have a great impact on several fields such as materials, i.e., nanomaterials for magnetic or electronic applications, and catalysis, where the location and microstructure of the deposited phase generally play a key role on the final properties of the materials. For detailed description on the different possibilities of electron tomography in the study of materials, several devoted reviews have already been published.[34−36]

However, it is noteworthy that the use of 3D TEM technique to study the nanoparticles located within the carbon nanotubes channel has not been so far reported despite the ever-increasing research effort devoted to this field, especially for catalytic applications.[26−28] Palladium-based catalysts supported on/in carbon nanotubes and carbon nanofibers have been reported to be highly active and selective catalysts for liquid-phase hydrogenation reaction[19,20,37,38] and thus, require more detailed characterizations in order to clarify the catalyst structure and the catalytic performance relationship. In the present work, we describe the use of TEM tomography to study the distribution and location of palladium particles with respect to the carbon nanotube channel as well as the influence of the inner diameter of the nanotube on the filling process. The influence of the oxygenated functional groups on the nanotube surface, generated by means of acidic treatment, on the filling behavior will also be discussed.

**Experimental Section.** *Support Material.* The carbon nanotubes were supplied by Applied Sciences Ltd. (Ohio). The carbon nanotubes have both ends opened and an average inner diameter varying from 15 to 30 nm and lengths up to several micrometers. The carbon nanotubes were treated at 80 °C in an aqueous solution of $HNO_3$ (67 vol %) for 14 h in order to remove the residual catalyst and to functionalize the nanotube surface for further deposition of the active phase.

*Catalyst Preparation.* The catalyst studied in the present work consists of palladium nanoparticles deposited by incipient wetness impregnation onto commercial multiwalled carbon nanotubes with a metal loading of 10 wt %. The palladium salt ($Pd(NO_3)_2$) was dissolved in an aqueous solution at room temperature. The carbon nanotubes were slowly dropped into the palladium solution until a pastelike solid was obtained. The impregnated solid was allowed to dry overnight at room temperature and was subsequently reduced in flowing hydrogen at 400 °C (heating rate of 2 $°C \cdot min^{-1}$) for 1 h in order to decompose the salt precursor

into its corresponding metal. The sample was left to cool to room temperature in flowing hydrogen, then the hydrogen flow was replaced by a mixture of $O_2$ (1 vol %) diluted in helium in order to passivate the metal surface before removing it from the reactor.

*Catalyst Characterization.* Conventional 2D TEM analysis was carried out on a Topcon 002B-UHR microscope working at 200 kV accelerating voltage with a point-to-point resolution of 0.18 nm. For TEM observation, the samples were ultrasonically dispersed in ethanol for 5 min, and a drop was deposited onto a holey carbon membrane copper grid.

The tilt series for 3D analysis were acquired in bright-field mode on a F20 TECNAI microscope (FEI Company) using an accelerated voltage of 200 kV and a high-tilt sample holder. Several series of 2D-TEM images were acquired using a 2048 pixel × 2048 pixel cooled CCD array detector in different places of the grid containing typical open-ended nanotubes. Each series of projections was collected over a tilt range of −65−65°, with an image recorded every 2° between −40° and 40° and every 1° elsewhere, giving a total of 91 images. During the acquisition, the TEM parameters such as defocus, horizontal specimen shift, and specimen tilt were controlled automatically. No evidence of irradiation damage in the sample was observed during the acquisition. Before acquisition of a tilt series of typical TEM images, a drop of a solution containing well-dispersed gold nanoparticles with a calibrated diameter of 5 or 10 nm was deposited onto the holey carbon grid supporting the sample to make the data treatment easier.

The tilt series data were treated for imaging processing and reconstruction using IMOD software program from the University of Colorado.[39] Before reconstruction, the views contained in a tilt series have to be aligned precisely with respect to each other in order to find a fixed axis tilt for the data set, the axis of which then passes through the center of the reconstruction volume. A rough alignment is first performed by the cross-correlation algorithm using the nominal tilt angles, where the Fourier transforms of subsequent images are compared and the result is a series of pre-aligned images. After that, a more precise alignment is carried out by using a least-squares tracking procedure of the position of gold nanoparticles dispersed on the grid supporting the sample. These markers are picked or automatically located on the pre-aligned images, and the program tests their positions and recommends changes in the values of tilt angles and tilt axis positions for each image. This test is crucial and has to be run many times in order to obtain a well aligned 2D image series with corrected tilt angles.

The volume reconstructions were then calculated from the aligned projection series using a back-projection technique,[40] the standard approach to tomographic reconstruction. Each 2D image is projected into a 3D reconstruction space back along the tilt angle at which this image was recorded. The superposition of these back-projected volumes from all projection yields to an approximation of the original object. A simple weighting filter is used in order to reduce the artifacts related to an uneven and incomplete sampling of angular range. Using the formula given by Midgley et al.[30] concerning the resolutions in tomograms, we have estimated the 3D spatial resolution with our geometrical parameters in data acquisition and characteristics of the specimen. In the direction perpendicular to the electron beam, the resolution was about 1.5−2 nm, whereas in the parallel direction, deterioration by a supplementary factor due to the limited tilt angle triggered a little lower resolution of about 2−2.5 nm.

There are two main possibilities to visualize and analyze the reconstructed volume. The first is the visualization and the analysis of 2D slices corresponding to transverse sections through the reconstruction. The slices are easily interpreted, but the overall visualization of the sample is more difficult due to its high 3D geometrical character. On the other hand, an accurate analysis of the nanoparticle size cannot be performed from an individual slice. The second way is the surface rendering of a well-defined object present in the reconstruction, i.e., to build a corresponding 3D model. To obtain it, preliminary steps are sometimes necessary in order to enhance the image contrast. Different contributions to the volume data are successfully separated, in our case the carbon nanotube, the Pd and Au nanoparticles, and the amorphous residual phase coming from the ethanol solution used to disperse the carbon nanotubes on the carbon grid. These contributions were obtained by selecting different bands of gray values of the voxels contained in the volume data (which correspond in fact to the different objects) and assigning them defined colors. The data segmentation process described above is followed by a surface rendering, and the resultant surfaces are finally displayed in a 3D model.

**Results and Discussion.** *Support Characterization.* The carbon nanotubes surface was also covered with numerous functional groups that were probably formed during the acidic treatment to remove the remaining catalyst.[41,42] It is well-known that all carbon forms are metastable against oxidizing agents, i.e., oxygen, nitric acid, sulfuric acid, aqua regia, etc. The reaction led to the formation of oxygen functional groups[43−45] with a wide variety, i.e., carboxylic acid, phenolic, acid anhydride, lactone, or quinoid (carbonyl), especially at low-temperature treatment, which is propitious to the formation of complex carbon oxygen groups.[46] The density of the oxygenated functional groups also tightly depends on the density of the defects on the carbon surface. These oxygenated groups interact with polar molecules and render more hydrophilic the treated carbon surface.[47,48] These groups can be clearly observed by the XPS spectrum recorded on the carbon nanotubes (Figure 1).

Classical TEM investigation carried out in bright-field mode on the raw material indicated the presence of a straight channel in the middle of the carbon nanotubes (Figure 2). Some encapsulated material corresponding probably to a residual phase can be also distinguished inside the channel (white arrows on the figure). The TEM analysis reveals also the presence of some graphite encapsulated iron-based catalysts that were not effectively removed during the acidic treatment. These iron-based particles were hermetically wrapped with several graphene layers and thus were not accessible for neither liquid nor gas-phase medium. Such

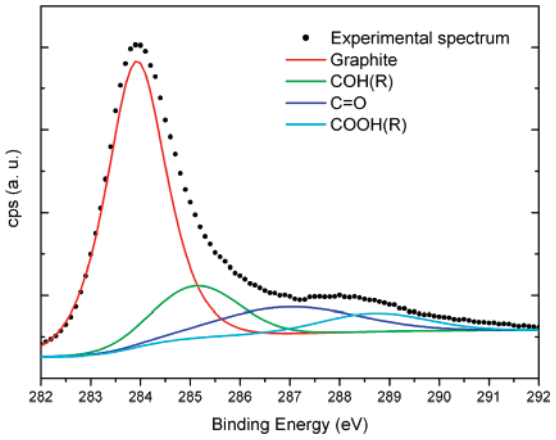


**Figure 1.** XPS C 1s spectrum showing the presence of several functional groups on the carbon nanotubes surface consecutive to the acidic treatment. These functional groups were expected to provide anchorage sites for the deposited metal active phase.

phenomenon is frequently observed in the case of carbon nanotubes grown from iron catalyst.[49,50] According to the work of Emmenegger and al.[50] an iron-based catalyst was encapsulated by graphite layers before reaching the critical dimension for growing carbon nanotube and thus become inactive for carbon nucleation sites.

*Pd/CNTs Characterization by 2D TEM.* In Figure 2B is presented a traditional 2D TEM of the sample. The palladium, i.e., small particles, seems to be homogeneously dispersed throughout the support. Round-shaped bigger particles were gold nanoparticles deposited on the sample for the final alignment of the 2D series images. However, because this image is only a 2D projection of the whole sample, one cannot attribute the exact location of the palladium particles with respect to the carbon nanotubes morphology, i.e., inside the channel or on the outer surface. The individual morphology (individual particles or aggregates) of the metal particle cannot be easily solved due to the low contrast of 2D images obtained by projecting a relatively thick 3D sample on a planar surface. The presence of trapped residues (coming from the ethanol employed as dispersant solvent) inside the carbon nanotube channel can be visible with, however, a relatively low contrast. TEM observation of the same samples (the CNT and the CNT with Pd particles) without sonication in the ethanol (dry deposition sample) clearly indicates the absence of such a meniscus inside the nanotube channel and thus confirms that these residues were formed during the drying process after the nanotubes were filled by ethanol during the sonication dispersion step.

High-resolution TEM investigation was also carried out in order to get more insight about the location of the palladium particles. The corresponding images are presented in Figure 3. However, due to the superimposition of the carbon nanotube wall and palladium particles, the distinction between the different palladium particles, especially those located next to or inside the nanotube channel, is not obvious. Only the particles located on the outer surface and well oriented with respect to the electron beam can be viewed accurately in HR-TEM (Figure 3). TEM analysis indicates that the dispersion was relatively high, as palladium particles were evenly distributed across the tube surface with an average particle size of ca. 5 nm in the case of the sample studied using this classical technique. This high dispersion was attributed to the presence of a large number of oxygenated functional groups on the nanotube surface, which provide anchoring sites for the supported species.[47,48] De Jong and co-workers[51] have reported during their study on the deposition of cobalt particles on the hollow carbon nanofibers surface that, without a postsynthesis acidic treatment to create surface oxygenated groups, the cobalt particle dispersion was relatively poor, i.e., 300 nm instead of 3−4 nm in the case of acidic treatment. Such observation could be directly linked to the low interaction between the nanofiber surface without oxygen functional groups and the deposited metal phase. The hydrophobic character of the carbon nanofibers without acidic treatment could be also responsible for this low dispersion due to the low surface wetting.

*Pd/CNTs Characterization by 3D TEM.* Examples of slices through the reconstructed volume are presented in Figure 4. These transverse sections through the sample are characterized by a contrast enhancement with respect to initial projections (a typical example is given in Figure 4A). However, we can observe in the transverse sections perpendicular to the tilt axis (Figure 4G) some lack in information, especially on the top and bottom parts of the object, due to the limited tilt angle, which induces a small blurring of the

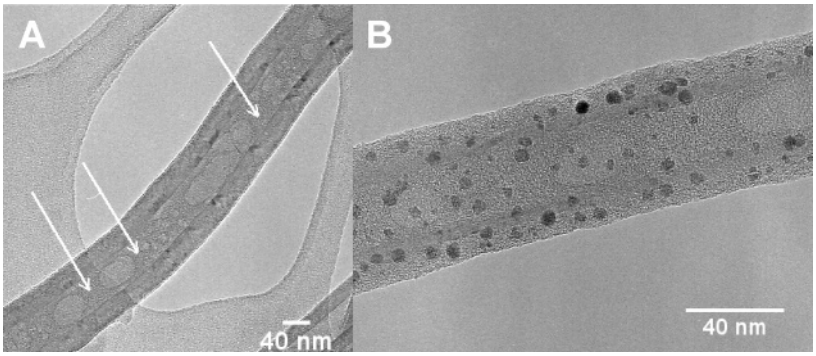


**Figure 2.** (A) Typical TEM image of a carbon nanotube showing its straight channel and also the presence of a foreign phase inside the tube indicated by arrows. (B) 2D TEM image of a Pd/MWNT. The projected image renders almost impossible the interpretation of the metal particles location and their microstructure along the thickness of the sample.

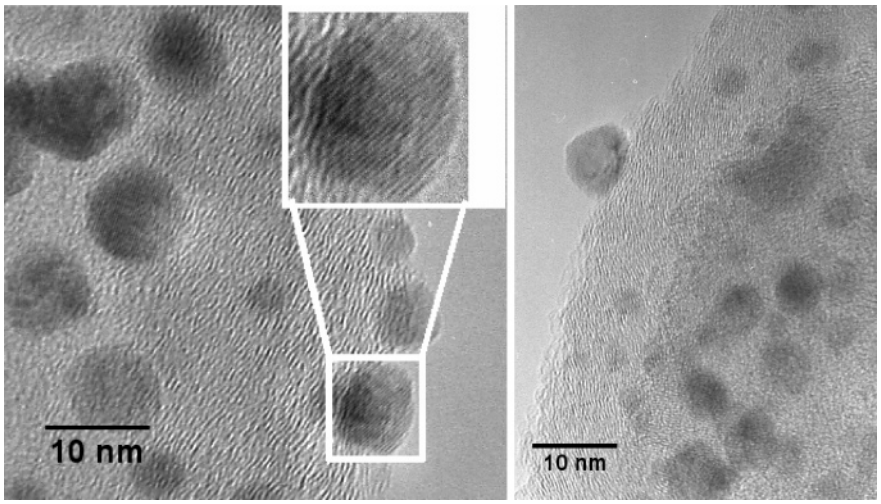


**Figure 3.** High-resolution 2D TEM micrographs of palladium supported on/in carbon nanotube. Only the Pd particles located on the outer surface can be visualized accurately.

reconstruction and thus a relatively bad definition of the boundaries of the nano-object in these areas.

A quick analysis of the reconstructed volume confirms the presence of individual metal particles instead of aggregates. Moreover, in the transverse sections, the presence of an amorphous phase was observed inside and also on the outer surface of the carbon nanotube (Figure 4F), but with a higher accuracy than with a 2D TEM image (taken into account the fact that the signal-to-noise ratio is higher in a section from the reconstructed volume than in a projection). The starting point of this residual phase was the ethanol solution used to disperse the carbon nanotubes on the TEM membrane grid in order to ease their observation. After air-drying, a soluble material, initially dissolved in ethanol solution, penetrates inside the tube or remains on the outer surface, keeping the memory of the wetting of two surfaces by the ethanol solution, as can be observed on the images (Figure 4B−E). Moreover, inside the nanotube channel, the transverse sections analysis highlights the presence of some elliptical air cavities trapped by this residual phase, that are much more visible once again with respect to 2D projections (Figure 4G). The presence of these air cavities as well as the very low contact angles between some of these cavities and the carbon wall indicate the high degree of wetting. Gogotsi and co-workers[52] have reported similar results during their study of the behavior of water inside open carbon nanopipes, with an average inner diameter of ca. 250 nm, formed by CVD inside the alumina porous membrane. The SEM and TEM studies revealed that the CNT wall was highly disordered and hydrophilic, which allowed easy filling by water. The authors have observed that, due to the imperfect circularity of their nanotubes, meniscuses with asymmetric faces were observed.

For visualization, surface renderings were obtained using a segmentation procedure from the reconstructed volume in order to select contributions from the carbon nanotube, the palladium and gold nanoparticles, and the residual phase. The model as obtained is presented in Figure 5. The carbon nanotube is highlighted in green, the residual layers from the ethanol solution, inside and outside, in pink, and the gold and palladium particles in red. According to the results obtained by counting the particles, more than 50% of the palladium particles observed in the reconstruction (with a diameter higher than our resolution limit, about 2−2.5 nm) were located within the channel of the nanotube. A qualitative analysis of the particle sizes shows the presence of two different populations of particles: one with the mean size of about $3 \pm 0.5$ nm, the second with a mean diameter of $4 \pm 0.5$ nm. We underline here that it is very difficult to perform a complete statistical analysis of the particle size because the errors bars are large due to the proximity of the resolution limits and to the blurring effect in the reconstruction. However, the analysis of the geometrical positions of the inside Pd nanoparticles shows that their distribution along the tube axis is relatively homogeneous, with a density of about 0.13 particles per nanometer.

The high efficiency for filling was attributed to the relatively large inner diameter of the tube and to the low surface tension of the solvent used for particle insertion, water with a surface tension of 72 $mN \cdot m^{-1}$, which favors the filling by capillarity forces. It has been reported elsewhere[53] that compounds with low surface tension ($<190$ $mN \cdot m^{-1}$) could wet graphite and allow a good filling. In Figure 6 is presented a planar projection from contributions of the Pd and Au particles obtained by data segmentation of the reconstructed volume. According to this image, the Pd particles were extremely homogeneous in size regardless of their location with respect to the tube surface. Similar observations have also been reported by Winter and al.[51] during their study of the deposition of Pt and Co particles on the hollow carbon nanofibers. Such a result indicates that the interaction between the tube surface, either outer or inner, and the deposited metal was mainly coming from the $\pi$ interaction with the graphene plane of the tube wall according to the literature.[54,55] The intrinsic properties of metals are generally altered due to the electronic interactions between the deposited metal and the $\pi$-electrons of graphite, especially when the diameter of the metal is smaller than 10 nm.[56−60]

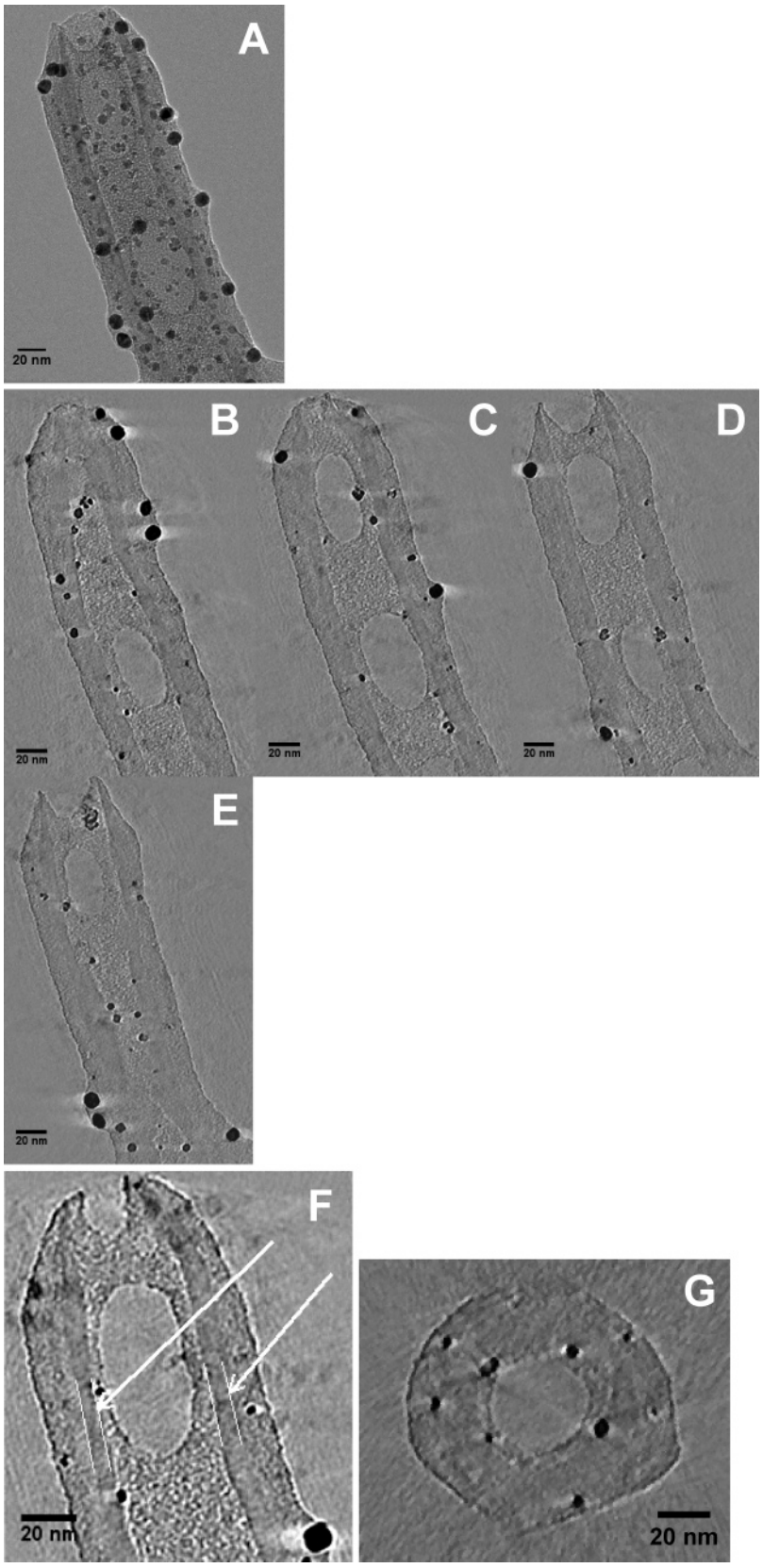


**Figure 4.** (A) Typical 2D TEM image (one of the projections of the object) from the tilt series used to reconstruct its volume. (B−E) Transverse sections through the reconstructed volume showing the location of the palladium particles along the carbon nanotube. The volume was obtained by reconstruction from a series of 91 classical electron microscopy images. The round-shaped particles with 10 nm in diameter are the gold particles deposited on the sample for 3D TEM calibration. (F) Section with a higher magnification to highlight the presence of an amorphous phase coming from ethanol inside the CNT channel and on its outer surface. (G) Transverse section perpendicular to the tube axis (which is parallel to the tilt axis) showing the good wetting of the inner tube wall by the liquidlike phase coming from ethanol solution.

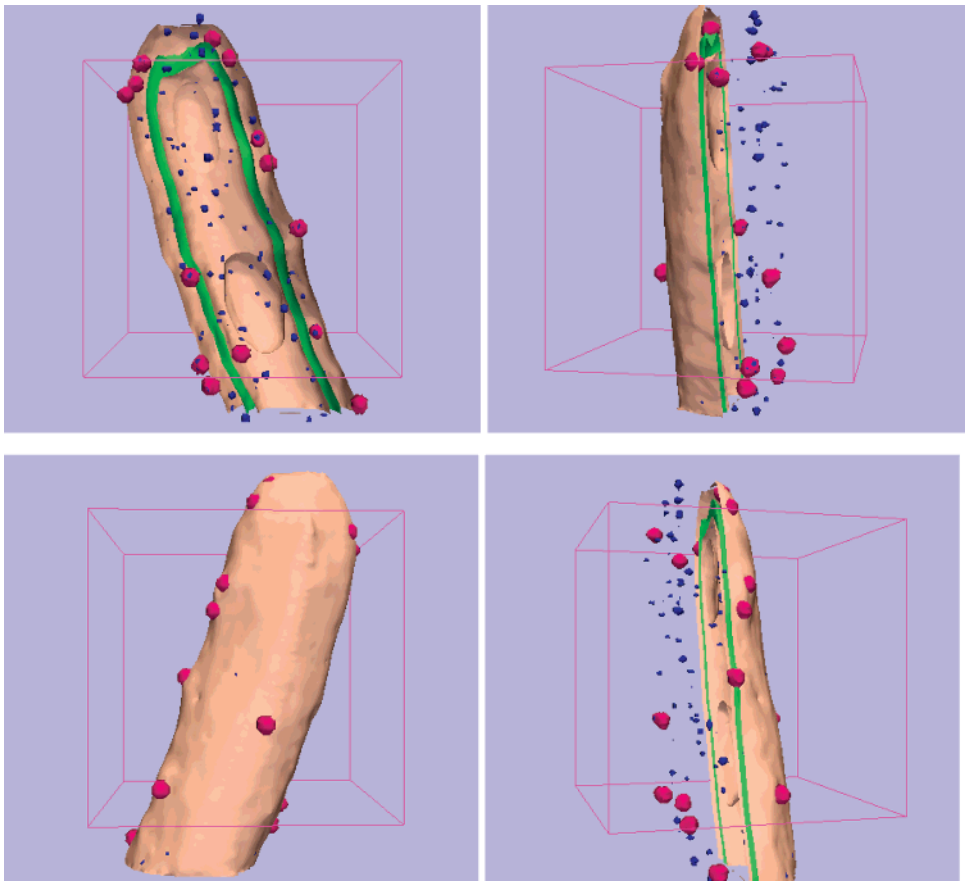

**Figure 5.** Views of a 3D reconstruction model of the Pd/MWNTC showing the high efficiency in filling of the nanotubes by palladium particles (in red, gold particles; blue, palladium particles; green, carbon nanotube; pink, amorphous residues from ethanol solution trapped inside the nanotube channel and on the outer surface).

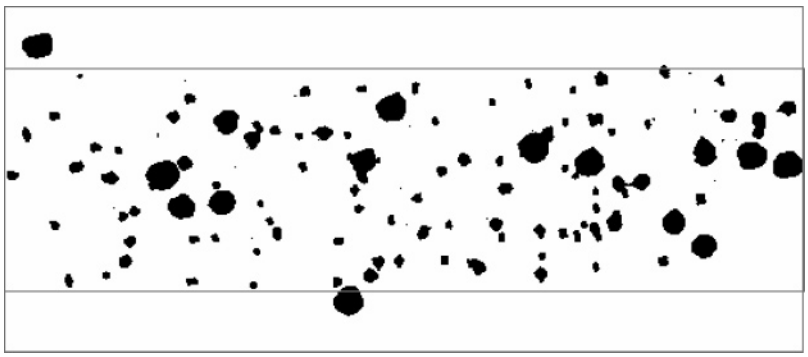

**Figure 6.** Planar projection acquired from the contributions of Pd (small particles) and Au (bigger particles) obtained by data segmentation of the reconstructed volume.

According to the wetting of the nanotube surface, it seems that both the outer and inner surfaces of the nanotube are similar in terms of hydrophilicity.

*Influence of the Inner Diameter on the Filling.* The behavior of fluids in nanotubes is expected to be greatly differing from the one occurring in traditional systems and to be strongly influenced by the inner diameter of the tube. To verify the influence of the diameter of nanotubes, a test was carried out on carbon nanotubes with a smaller diameter, i.e., 15 nm instead of 30 nm. A typical 2D image recorded in high angle annular dark-field mode (HAADF) is presented in Figure 7. Again, the 2D character of as obtained images renders less obvious the attribution of the palladium particles location with respect to the CNT channel.

To get more insight about the exact location of the metal particles, a 3D analysis was carried out from a tilt series recorded in HAADF mode using the same treatment as described before (for the sample with 30 nm inner diameter). We decided here to use the STEM-HAADF mode for the acquisition of the tilt series in order to improve the quality of the reconstruction of Pd nanoparticles in the calculated volume of the whole object. In this particular mode, the images are recorded in scanning mode and they are strongly dependent on the atomic number of the components (*Z*-

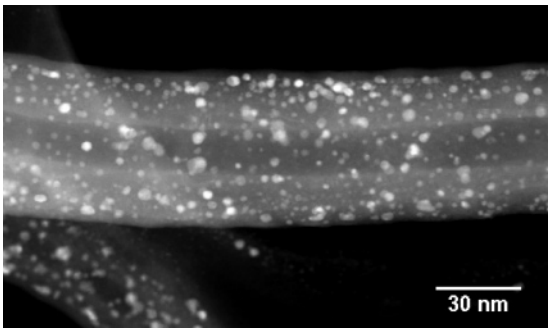


**Figure 7.** Typical STEM-HAADF image from the tilt series recorded for 3D analysis on a carbon nanotube with an inner diameter of 15 nm and palladium particles deposited on the outer surface.

contrast imaging). Therefore, there is a tremendous improvement in contrast and clarity in the reconstruction of the Pd particles (heavy atoms) with respect to the carbon nanotube and residual phase (light atoms). Consequently, the observation and analysis of the Pd nanoparticles become more efficient. A view of the 3D model obtained by selecting particles contributions is presented in Figure 8A and shows the homogeneity in size of Pd nanoparticles (the bigger particles are gold beads) that can be evidenced in the reconstruction, within our resolution limits of 2−2.5 nm. Two orthogonal views of the 3D models corresponding to both carbon nanotube and particles are also presented in Figure 8B and C. Looking along the tube axis, one can easily observe the location of the Pd particles with respect to the CNT inner surface (represented by black circle in Figure 8B−D). In the case of tubes with smaller diameters, the filling percentage was almost nil instead of more than 50% for the tubes with larger diameters (Figure 8D), once again within a resolution limit of about 2−2.5 nm. Decreasing the inner diameter from 30 to 15 nm led to a significant drop in filling, almost resulting in the exclusive deposition of palladium particles on the outer wall of the carbon nanotubes.

It is thought that with smaller diameter the capillarity forces were not strong enough to allow the complete filling of the tube, leading to a significantly lower amount of metal particles inside the inner channel. Ma and al.[61] have reported results on platinum filling into carbon nanotube with two different inner diameters, i.e., <10 nm and 60−100 nm, using an incipient wetness method with an alcoholic solution of platinum salt. The authors have observed that a complete filling was occurring with nanotubes having an inner diameter of 60−100 nm, whereas no filling at all was happening with a tube of smaller inner diameter despite the use of a relatively low surface tension solvent such as ethanol. Apparently, a tube with a small inner channel inhibits the filling by simple capillarity at mild conditions. The observed results also explain why most of the filling studies by capillarity have been conducted with carbon nanopipes with diameter over 100 nm.

Ugarte and al.[62] have reported that the capillarity of narrow nanotubes is significantly reduced with respect to large inner diameter and cavity size. During the filling process, the van der Walls forces dominating the liquid−solid interactions

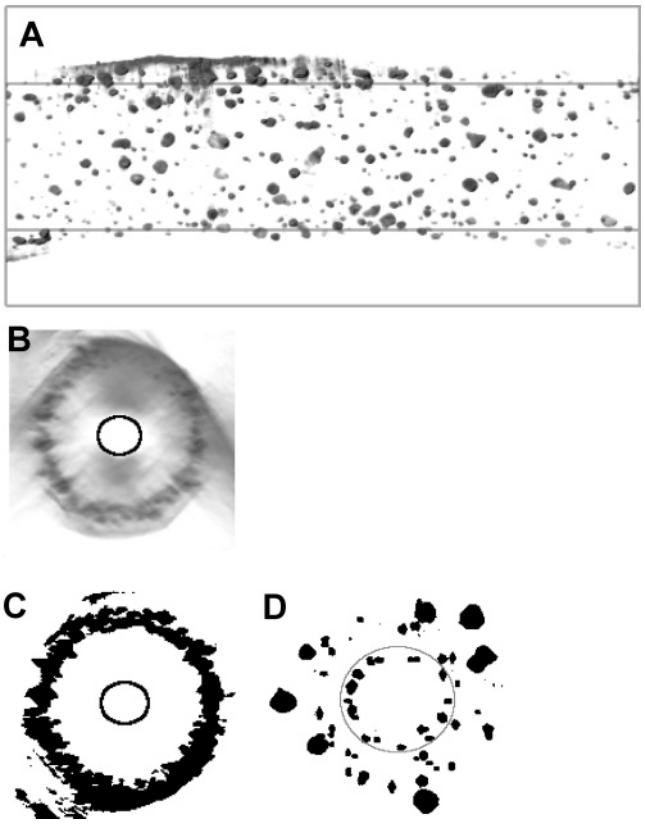


**Figure 8.** Three-dimensional models obtained from the reconstructed volume on a carbon nanotube with an inner diameter of about 15 nm. (A) View of 3D model obtained by selecting only the Au and Pd nanoparticles contribution from the reconstruction. (B) View along the tube axis of both nanoparticles and carbon nanotube contributions. (C) View along the tube axis of the 3D model corresponding to palladium nanoparticles only (nanotube with 15 nm diameter). (D) View along the tube axis of the 3D model representing the gold and palladium nanoparticles for the carbon nanotube with inner diameter of 30 nm. In Figures B, C, and D, the inner surfaces of the tubes are indicated by circles.

strongly depend on the polarizability of the wetted materials. The polarizability of the concave graphite surface (inner wall) is noticeably reduced compared to a planar graphite surface and is determined by the diameter of the cavity. It is expected that, under a certain value of inner diameter, almost no filling should happen under our filling conditions, i.e., room temperature with aqueous solution, resulting in a competitive deposition of the metal particles on the outer surface of the nanotube. Some published works[63] have reported that carbon nanotubes with small inner diameter could be filled under more drastic conditions. Sloan and Green have recently reported interesting results using vacuum diffusion or high-temperature processes with either molten salts or acidic medium.[64] Carbon nanotubes with very small inner diameter, i.e., 2 to 5 nm, can also be efficiently filled by water under high pressure and temperature treatments in an autoclave. Water was slowly filled inside the nanotube through defects present along the tube wall during the hydrothermal treatment.

However, the diameter of the palladium particles was not affected by their location, in or out of the nanotube. Moreover, the amorphous residues were observed on both

inner and outer surfaces with a high degree of wetting. That indicates that the nature of two surfaces of the nanotube were similar (surface decorated by oxygenated groups such as −COOH, −COO, −OH, etc. during the postsynthesis acidic treatment in order to remove the iron catalyst). Similar observations were also reported by de Jong and co-workers[51] during their study on palladium and cobalt particles deposited on the hollow carbon nanofibers.

According to their results, carbon nanotubes with an inner diameter at least equal to 30 nm can be successfully filled with foreign elements under mild conditions. Decreasing the diameter of the channel led to a less efficient filling as the van der Walls interactions were less active.

**Conclusion.** According to 3D-TEM analysis, the filling of carbon nanotubes by Pd nanoparticles using the capillarity under mild conditions, i.e., aqueous solution and room temperature, was strongly dependent on the inner diameter of the tube: a filling efficiency of about 50% can be achieved with tube having an inner diameter of ca. 30 nm, whereas it became almost nil when the inner diameter of the tube was decreased from 30 to 15 nm, within the resolution limit of the technique in our experimental conditions, i.e., about 2 nm. Apparently, with small inner diameter, the repulsion forces are stronger and thus fluid penetration by capillarity is no longer observed.

The use of 3D-TEM technique is here crucial: it allows one to obtain precisely the positions of nanoparticles with respect to the carbon nanotube support and to calculate the efficiency of the filling process. Moreover, if the nanotube is filled or surrounded by a residual phase coming from a liquid solution, the analysis of transverse sections of the reconstructed volume allows one to obtain useful information about the morphology of this complex system as well as the wetting of the tube by the initial solution.

Three-dimensional TEM also allows one to confirm that, after acidic treatment, both surfaces of the nanotube were similar in nature, leading to a high dispersion of the Pd particles with narrow size distribution. Similar results were also observed in the case of filled $CoFe_2O_4$ or $NiFe_2O_4$ nanowires as a function of the tube diameter. Work is ongoing to use 3D TEM to study the magnetic nanowires casted inside carbon nanotubes in order to get more insight about the real morphology and porosity of these nanowires.

In conclusion, one can state that 3D-TEM technique can be an extremely useful technique to get access to the morphology and location of metal nanoparticles within a support, in particular in the case of carbon nanotubes, and to thus provide more insight on the correlation between the macroscopic properties of the material and its nanoscopic structure. It can also be extremely efficient to estimate the wetting behavior of liquid after filling the nanotube channel, which could have a significant impact on the formation of filling compounds during thermal treatment. It is thought that such a technique could also be widely employed for other nanoscopic tubular structured materials that become more and more involved in the field of nanotechnology.

**Acknowledgment.** Three-dimenstional TEM experiments using the TECNAI microscope were carried out at the Institut de Génétique et de Biologie Moléculaire et Cellulaire de Strasbourg (IGBMC). We thank C. Crucifix for help during acquisition. The dark-field TEM studies were performed on a JEOL-JEM-2100F microscope by E. Okunichi and N. Endo at Akishima (Tokyo).

**Supporting Information Available:** Supporting figures and movies of the recorded tilt series, consecutive slices through volume reconstruction and 3D models of samples with inner diameter of 30 and 15 nm are available (AVI). This material is available free of charge via the Internet at http://pubs.acs.org.

## References

(1) Ebbesen, T. W. *Carbon Nanotubes: Preparation and Properties*; CRC Press: Boca Raton, FL,1997.
(2) Dai, H. *Acc. Chem. Res.* **2002**, *35*, 1035−1044.
(3) Lau, A. K.-T.; Hui, D. *Composites, Part B* **2002**, *33*, 263−277.
(4) Ledoux, M.-J.; Pham-Huu, C. *Catal. Today* **2005**, *102*−*103*, 2−14.
(5) Ebbesen, T. W.; Ajayan, P. M. *Nature* **1992**, *358*, 220−222.
(6) Guo, T.; Nikolaev, P.; Thess, A.; Colbert, D. T.; Smalley, R. E. *Chem. Phys. Letters* **1995**, *243*, 49−54.
(7) Kong, J.; Cassell, A. M.; Dai, H. *Chem. Phys. Lett.* **1998**, *292*, 567−574.
(8) Zhou, O.; Shimoda, H.; Gao, B.; Oh, S.; Fleming, L.; Yue, G. *Acc. Chem. Res.* **2002**, *35*, 1045−1053.
(9) Libera, J.; Gogotsi, Y. *Carbon* **2001**, *39*, 1307−1318.
(10) Gogotsi, Y.; Naguib, N.; Libera, J. A. *Chem. Phys. Lett.* **2002**, *365*, 354−360.
(11) Pederson, M. R.; Broughton, J. Q. *Phys. Rev. Lett.* **1992**, *69*, 2689.
(12) Ajayan, P. M.; lijima, S. *Nature* **1993**, *361*, 333−334.
(13) Ye, H.; Naguib, N.; Gogotsi, Y.; Yazicioglu, A. G.; Megaridis, C. M. *Nanotechnology* **2004**, *15*, 232−236.
(14) Ajayan, P. M.; Colliex, C.; Lambert, J. M.; Bernier, P.; Barbedette, L.; Tence, M.; Stephan, O. *Phys. Rev. Lett.* **1994**, *72*, 1722.
(15) Tsang, S. C.; Chen, Y. K.; Harris, P. J. F.; Green, M. L. H. *Nature* **1994**, *372*, 159−162.
(16) Chen, Y. K.; Chu, A.; Cook, J.; Green, M. L. H.; Harris, P. J. F.; Heesom, R.; Humphries, M.; Sloan, J.; Tsang, S. C.; Turner, J. F. C. *J. Mater. Chem.* **1997**, *7*, 545−549.
(17) Chen, Y. K.; Green, M. L. H.; Tsang, S. C. *Chem. Commun.* **1996**, *21*, 2489−2490.
(18) Ebbesen, T. W. *J. Phys. Chem. Solids* **1996**, *57*, 951−955.
(19) Tessonnier, J.-P.; Pesant, L.; Ehret, G.; Ledoux, M. J.; Pham-Huu, C. *Appl. Catal., A* **2005**, *288*, 203−210.
(20) Nhut, J.-M.; Nguyen, P.; Pham-Huu, C.; Keller, N.; Ledoux, M.-J. *Catal. Today* **2004**, *91*−*92*, 91−97.
(21) Toebes, M. L.; Prinsloo, F. F.; Bitter, J. H.; van Dillen, A. J.; de Jong, K. P. *J. Catal.* **2003**, *214*, 78−87.
(22) Pham-Huu, C.; Keller, N.; Estournes, C.; Ehret, G.; Greneche, J. M.; Ledoux, M. J. *Phys. Chem. Chem. Phys.* **2003**, *5*, 3716−3723.
(23) Tessonnier, J. P.; Wine, G.; Estournes, C.; Leuvrey, C.; Ledoux, M. J.; Pham-Huu, C. *Catal. Today* **2005**, *102*−*103*, 29−33.
(24) Pham-Huu, C.; Keller, N.; Ehret, G.; Ledoux, M. J. *J. Catal.* **2001**, *200*, 400−410.
(25) Nhut, J.-M.; Pesant, L.; Tessonnier, J.-P.; Winé, G.; Guille, J.; Pham-Huu, C.; Ledoux, M.-J. *Appl. Catal., A* **2003**, *254*, 345−363.
(26) Koster, A. J.; Ziese, U.; Verkleij, A. J.; Janssen, A. H.; de Jong, K. P. *J. Phys. Chem. B* **2000**, *104*, 9368−9370.
(27) Gommes, C. J.; de Jong, K.; Pirard, J. P.; Blacher, S. *Langmuir* **2005**, *21*, 12378−12385.
(28) Janssen, A. H.; Yang, C. M.; Wang, Y.; Schuth, F.; Koster, A. J.; De Jong, K. P. *J. Phys. Chem. B* **2003**, *107*, 10552−10556.
(29) Weyland, M.; Midgley, P. A.; Thomas, J. M. *J. Phys. Chem. B* **2001**, *105*, 7882−7886.
(30) Midgley, P. A.; Weyland, M. *Ultramicroscopy* **2003**, *96*, 413−431.
(31) Thomas, P. J.; Midgley, P. A. *Ultramicroscopy* **2001**, *88*, 179−186.
(32) Thomas, P. J.; Midgley, P. A. *Ultramicroscopy* **2001**, *88*, 187−194.
(33) Grimm, R.; Typke, D.; Baumeister, W. *J. Microsc.* **1998**, *190*, 339−349.
(34) de Jong, K. P.; Koster, A. J. *ChemPhysChem* **2002**, *3*, 776−780.
(35) Mobus, G.; Doole, R. C.; Inkson, B. J. *Ultramicroscopy* **2003**, *96*, 433−451.

(36) Deans, S. R. *The Radon Transform and Some of Its Applications*; Wiley: Chichester, U.K., 1983.
(37) Pham-Huu, C.; Keller, N.; Ehret, G.; Charbonniere, L.; Ziessel, R.; Ledoux, M. J. *Chem. Commun.* **2000**, *19*, 1871−1872.
(38) Pham-Huu, C.; Keller, N.; Ehret, G.; Charbonniere, L. J.; Ziessel, R.; Ledoux, M. J. *J. Mol. Catal. A: Chem.* **2001**, *170*, 155−163.
(39) Mastronarde, D. N. *J. Struct. Biol.* **1997**, *120*, 343−352.
(40) Weyland, M. *Top. Catal.* **2002**, *21*, 175−183.
(41) Kuznetsova, A.; Popova, I.; Yates, J. T.; Bronikowski, M. J.; Huffman, C. B.; Liu, J.; Smalley, R. E.; Hwu, H. H.; Chen, J. G. *J. Am. Chem. Soc.* **2001**, *123*, 10699−10704.
(42) Kyotani, T.; Nakazaki, S.; Xu, W.-H.; Tomita, A. *Carbon* **2001**, *39*, 782−785.
(43) Delannay, F.; Tysoe, W. T.; Heinemann, H.; Somorjai, G. A. *Carbon* **1984**, *22*, 401−407.
(44) Kelemen, S. R.; Freund, H.; Mims, C. A. *J. Catal.* **1986**, *97*, 228−239.
(45) Schlögl, R. *Handbook of Porous Solids*; Wiley-VCH: New York, 2002.
(46) Yang, J.; Mestl, G.; Herein, D.; Schlogl, R.; Find, J. *Carbon* **2000**, *38*, 715−727.
(47) Toda, T.; Igarashi, H.; Uchida, H.; Watanabe, M. *J. Electrochem. Soc.* **1999**, *146*, 3750−3756.
(48) Sun, X.; Stansfield, B.; Dodelet, J. P.; Desilets, S. *Chem. Phys. Lett.* **2002**, *363*, 415−421.
(49) Ermakova, M. A.; Ermakov, D. Y.; Chuvilin, A. L.; Kuvshinov, G. G. *J. Catal.* **2001**, *201*, 183−197.
(50) Emmenegger, C.; Bonard, J. M.; Mauron, P.; Sudan, P.; Lepora, A.; Grobety, B.; Zuttel, A.; Schlapbach, L. *Carbon* **2003**, *41*, 539−547.
(51) Winter, F.; Leendert Bezemer, G.; van der Spek, C.; Meeldijk, J. D.; Jos van Dillen, A.; Geus, J. W.; de Jong, K. P. *Carbon* **2005**, *43*, 327−332.
(52) Rossi, M. P.; Ye, H.; Gogotsi, Y.; Babu, S.; Ndungu, P.; Bradley, J. C. *Nano Lett.* **2004**, *4*, 989−993.
(53) Dujardin, E.; Ebbesen, T. W.; Hiura, H.; Tanigaki, K. *Science* **1994**, *265*, 1850−1852.
(54) Park, C.; Keane, M. A. *J. Catal.* **2004**, *221*, 386−399.
(55) Salman, F.; Park, C.; Baker, R. T. K. *Catal. Today* **1999**, *53*, 385−394.
(56) Ma, J.; Rodriguez, N. M.; Vannice, M. A.; Baker, R. T. K. *J. Catal.* **1999**, *183*, 32−44.
(57) Kim, J.-H.; Suh, D. J.; Park, T.-J.; Kim, K.-L. *Appl. Catal., A* **2000**, *197*, 191−200.
(58) Bradford, M. C. J.; Vannice, M. A. *Appl. Catal., A* **1996**, *142*, 73−96.
(59) Pierson, H. O. *Handbook of Carbon, Graphite, Diamond and Fullerenes*; Noyes: Park Ridge, NJ, 1993.
(60) Mattia, D.; Bau, H. H.; Gogotsi, Y. *Langmuir* **2006**, *22*, 1789−1794.
(61) Ma, H.; Wang, L.; Chen, L.; Dong, C.; Yu, W.; Huang, T.; Qian, Y. *Catal. Commun.* **2007**, *8*, 452−456.
(62) Ugarte, D.; Stöckli, T.; Bonard, J. M.; Châtelain, A.; de Heer, W. A. *Appl. Phys. A: Mater. Sci. Process.* **1998**, *67*, 101−105.
(63) Loiseau, A.; Willaime, F. *Appl. Surf. Sci.* **2000**, *164*, 227−240.
(64) Thamavaranukup, N.; Hoppe, H. A.; Ruiz-Gonzalez, L.; Costa, P. M. F. J.; Sloan, J.; Kirkland, A.; Green, M. L. H. *Chem. Commun.* **2004**, 1686−1687.

NL070529V